

Space Rider

Aerodynamics and Aerothermodynamics

from hypersonic to subsonic flight



Olivier LAMBERT and Marie-Christine BERNELIN***

**Dassault Aviation, Saint-Cloud, France*

olivier.lambert@dassault-aviation.com

***Dassault Aviation, Saint-Cloud, France*

marie-christine.bernelin@dassault-aviation.com

Abstract

This paper summarizes aerodynamic and aerothermodynamic studies conducted in the frame of Space Rider program. Building on IXV heritage, which successfully flew on February, 11th 2015, IXV aeroshape “*as-it-is*” has been elected as a suitable candidate capable of fulfilling Space Rider new mission requirements. Flight domain has been extended to transonic and subsonic Mach numbers thanks to WTT conducted at INCAS trisonic facility in Bucharest, Romania. For the hot part of the reentry, in order to counterbalance a significantly higher mass for Space Rider than for IXV, IXV flight data analyses have been conducted to allow thermal margins policy revision.

1. Introduction

Space Rider aims to provide Europe with an affordable, independent, reusable end-to-end integrated space transportation system for routine access and return from low earth orbit. It will transport payloads for an array of applications, orbit altitudes and inclinations. The Space Rider will be launch on VEGA-C and land smoothly and safely on ground thanks to Descent and Recovery System based on piloted parafoil. The Space Rider will be able to stay in orbit up to two months and will be reusable.

The Space Rider vehicle design inherits from technology developed for the ESA IXV vehicle which performed a successful aero-controlled atmospheric re-entry trajectory on the 11th of February 2015. A preliminary IXV Post-Flight analysis demonstrated that the flight was nominal. The first flight reconstruction shows a very good prediction of the aerodynamic behavior and a conservative prediction of the thermal loads observed during the flight.

As for IXV project, Dassault-Aviation is leader of the AED-ATD team in charge of the aeroshape consolidation and of the AED and ATD databases. This paper presents the state of the art of the Aerodynamics and Aerothermodynamics activities.

2. Aerodynamics

During first phase A/B1 of Space Rider program (2016-2017), building on previous IXV aerodynamic studies, IXV “as-it-is” aeroshape’s capability to fly safely through supersonic, transonic and subsonic regime down to Mach=0.6 was evaluated, to verify its eligibility to fulfill Space Rider mission requirements.

Supersonic to subsonic flight envelope extension has been conducted thanks to a first WTT campaign conducted at INCAS trisonic facility in Bucharest, Romania in 2017. A full aerodynamic characterization in the range Mach = 1.4 to Mach = 0.6 has been completed, including longitudinal and lateral behavior (AoA and AoS effects), together with multiple symmetrical and asymmetrical flap deflections. Figure 1 shows a Schlieren visualization performed at Mach = 1.4 during these tests.



Figure 1: Space Rider WTT at INCAS trisonic facility - Mach = 1.4 AoA = 60 deg

Thanks to the data acquired during INCAS 2017 WTT campaign, IXV’s aerodatabase was extended to subsonic regime to create a first version of Space Rider AEDB. Flying qualities analyses were conducted with this aerodatabase in order to evaluate longitudinal and lateral stability and controllability in the transonic flight domain.

Figure 2 illustrates longitudinal behavior analysis: on the left hand side, pitching moment coefficient evolutions vs. AoA at different Mach number (from M=2 to M=0.6, zero flap deflection) illustrates that stability AoA range (negative C_m (AoA) slope) is moving to high and even very high AoA (more than 65 deg) when Mach number is decreasing. This behavior is confirmed for non-zero longitudinal flap deflections (Figure 2 right hand side): trim AoA (i.e. at $C_m=0$) for different longitudinal flap deflection is increasing from 45 deg at M=2 up to around 70 deg at M=0.6. And since for -10 to +10 deg flap setting, the same trend is observed, it was decided to follow the natural aerodynamic behavior by choosing an increasing AoA profile strategy to fly through transonic, keeping longitudinal flap deflection close to zero, trying this way to maximize the remaining flap authority for lateral control.

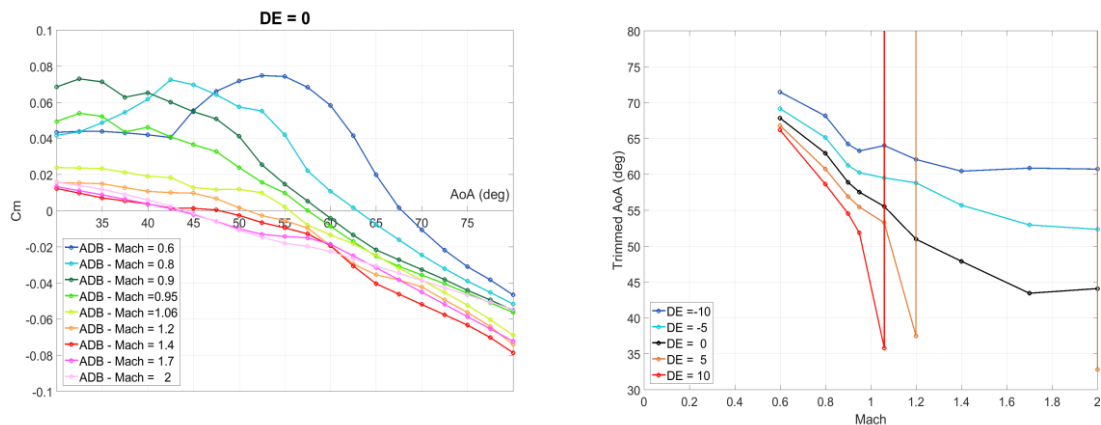


Figure 2: Space Rider AEDB: Pitching moment coefficients vs. AoA in supersonic and transonic (left), and AoA profile for different longitudinal trim (right)

Regarding lateral behavior, Figure 3 presents the evolution of static yawing stability with the $C_{n\beta}$ vs. AoA : as for longitudinal stability, lateral stability AoA range (positive $C_{n\beta}$) is moving to high AoA when Mach number is decreasing. Dashed black line with triangles shows static lateral stability for trimmed AoA at zero elevon deflection: lateral stability remains quite constant when passing through transonic following the defined increasing AoA profile.

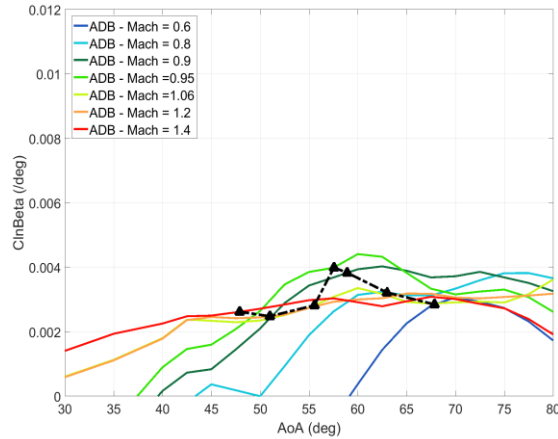


Figure 3: Static lateral yawing stability vs. AoA

The so-built aerodatabase has been delivered to DEIMOS and SENER to be used for their Guidance, Navigation and Control analyses and for mission analysis. One of the preliminary conclusions of these studies is that flap authority needed to pass through transonic can sometimes be saturated if aileron deflection is limited to ± 10 deg, that is why a complementary WTT campaign has recently been conducted during current Phase B2/C to complete flap efficiencies for high aileron deflection (up to 20 deg), aiming to improve robustness of the Guidance, Navigation and Control strategy in the transonic Mach range. Figure 4 illustrates elevon (DE) and aileron (DA) deflections available for the different combinations of Left and Right flap deflections; dashed blue line presents the current validity domain for flap deflections in the AEDB, and shows that lateral authority can be improved at low longitudinal deflection by completing AEDB with the pink red circles for the different Mach numbers from $M=1.4$ to $M=0.6$.

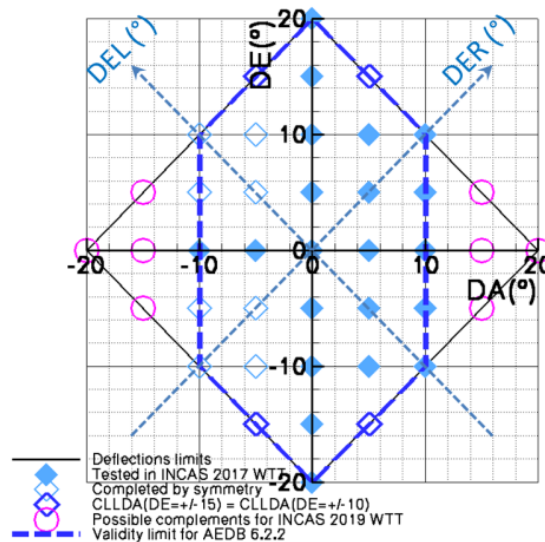


Figure 4: Longitudinal and lateral flap authority elevon/aileron DE/DA vs. Left/Right flap deflection

Another important topic to ensure aerodynamic is safe flying through transonic regime is the identification of damping coefficients for pitching behavior, since several studies have shown some potential dynamic instabilities for such aerospace flying through transonic.

Damping derivatives consolidation has thus been conducted through unsteady CFD computations performed by CFSe in previous phase A/B1. Forced pitching and plunging oscillations have been computed for 4 Mach numbers, allowing the quantification respectively of $(C_{mq} + C_{m\alpha\dot{\alpha}})$ and $C_{m\alpha\dot{\alpha}}$. Figure 5 shows pitching moment coefficient time history for pitching oscillations computations (left), and the coefficient finally extracted from these computations to be put in the aerodatabase (right).

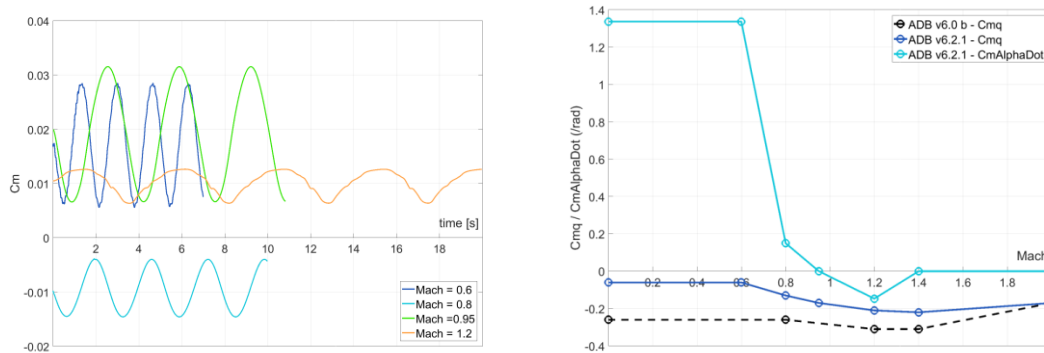


Figure 5: CFSe forced pitching oscillations time history

During current phase B2/C, consolidation of these values is conducted through unsteady CFD computations performed by INCAS in the same conditions as the ones previously performed by CFSe, and also thanks to dynamic oscillations WTT performed in S1 wind tunnel in VKI which are planned in July 2019: Figure 6 shows a global view of the mounting and oscillating mechanism designed by VKI for these tests.

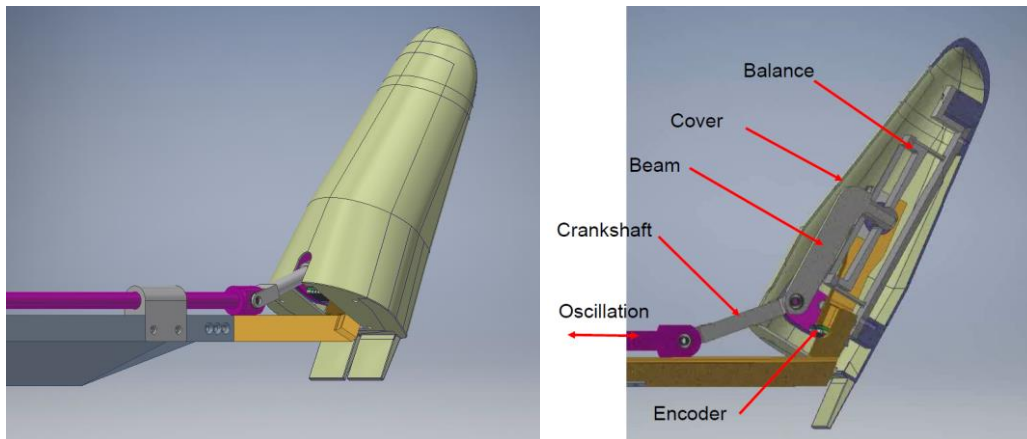


Figure 6: VKI S1 WTT mounting for forced pitching oscillations

3. Aerothermodynamics

As a first attempt, the IXV vehicle aims to validate the design tools, Guidance Navigation and Control, various technologies (TPS, structure, RCS, DRS, etc) and system verification involved in aero-controlled re-entry hypersonic vehicle. The vehicle was a flying testbed integrating an In-Flight Experimental plan to better understand the various aerothermodynamics phenomena observed during an atmospheric re-entry trajectory and aiming to validate ground prediction tools.

Experiment Number	Experiment	Category	Req	AED/ATD Priority	Phenomena	Area	Remarks
8	SWALL	AED-ATD	50_R1010_R108 150_R180_250_R1 R010	1/24	Real gas effects. Shock-wave boundary layer interaction. Flap surface efficiency-ATD	Flap/Hinge	Flap is well instrumented to cover the experiment but the phenomenon could not happen, depending on deflection angle -CFD sensors mounted.
11.1	Continuous Flow - 1	AED-ATD	50_R18012	8	Ratified and continuous aerodynamic	Windward Flap Chin/Sub-08	
11.2	High Altitude AD - 2	AED-ATD	50_R18012	8	Ratified and continuous aerodynamic	Inside vehicle	
11.3	Base Flowfield - 3	AED-ATD	50_R180150_R18 011	1/7	Real gas effects. Base AED and ATD	Base	
11.5	Ground Heating - 5	AED-ATD	50_R1010_R108 150_R1804	1/5	Real gas effects. Turbulent heating	Whole vehicle surface	
11.6	Wall analysis - 6/8	AED-ATD	50_R180150_R18 018	1/10	Real gas effects. Material catalytic behavior	Windward	
11.7	Flap Temperature - 7	AED-ATD	50_R180150_R18 0150_R180150 R180500_R18010	1/8/11/2	Real gas effects. Shock-wave boundary layer interaction. Shock-shock interaction. Transitional separation. Flap surface efficiency-ATD	Flap	
11.8	No Kinetic interaction - 8	AED-ATD	50_R18011	8	RCS efficiency	Base	
11.9	LAT sensors - 9	AED-ATD	50_R1804	6	Laminar to turbulent transition	Windward Chin	
57	IF Camera/Truss Mapping	AED-ATD	50_R14550_R180 150_R180_250_R1 R0350_R180_550 -R18010	1/2/3/1/2	Real gas effects. Shock-wave boundary-layer interaction. Shock-shock interaction. Transitional separation. Flap surface efficiency and ATD	Flap	risk of pollution and overheating
10	Nose Cap	TPS	50_R10050_R110		Material Verification	Nose	
41	Abblative TPS	TPS	50_R025		Material Verification	Leeward Base	
24	Hinge joint	TPS	50_R100		Material Verification	Hinge	
28	Large Shingle	TPS	50_R110		Material Verification	Windward	
30	TPS junction	TPS	50_R10050_R140		Material Verification	Windward	
31.1	C/SAC Shingles	TPS	50_R10050_R110		Material Verification	Windward	
31.2	C/SAC Leading Edges	TPS	5_R10050_R110		Material Verification	Leading Edge	
40	Body Flap	TPS	50_R110		Material Verification	Flap	
12	CMC FADS	AED-ATD	50_R1801250_R2 1050_R220	8	Continuous aerodynamic	Nose	The quality of experiment depends on extra ground calibration effort
13.10	Cavity and cavity heating - 10	AED-ATD	50_R1807	12	Cavity heating	Windward Flap	
36	SFS Chip Flare and Skin Friction Sensors	AED-ATD	50_R18012	8	Ratified and continuous aerodynamic	Windward	substitution with OTS sensors

Figure 7: In-flight experiment for ground prediction tools validation

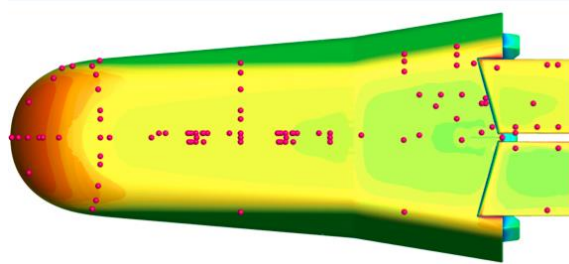


Figure 8: IFE – Pressure taps and thermocouple location at windward side

Even if the Space Rider aerodynamics is the same as the IXV one, the Space Rider mission leads to increase the total mass of the vehicle inducing higher heat flux during atmospheric re-entry. Thanks to the IXV flight data, a Post-Flight analysis was carried out enabling to refine and update the margins policy to be applied to Space Rider application.



Figure 9: IXV

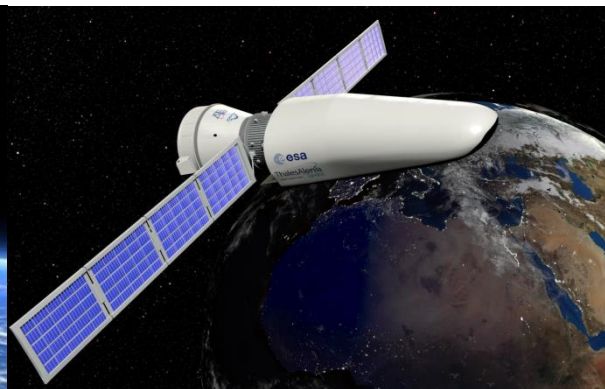


Figure 10: Space Rider

Using the flight re-entry trajectory as input, the AeroThermodynamic DataBase (ATDB) provides the sizing and reference heat fluxes (as shown on Figure 13).

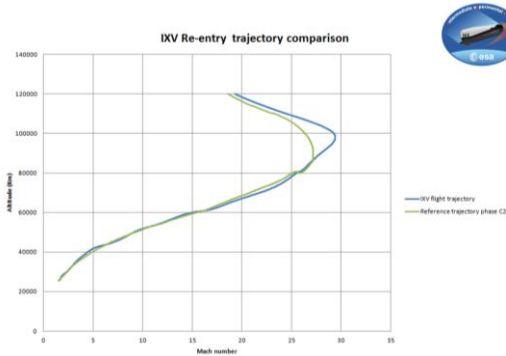


Figure 11: IXV reference and flight re-entry trajectories

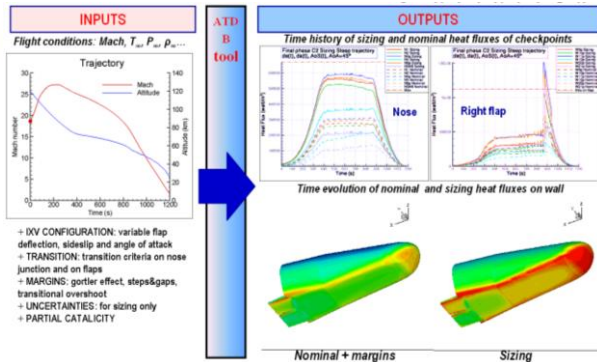


Figure 12: AErothermodynamic DataBase, ATDB

The Figure 11 shows a comparison with the flight re-entry trajectory demonstrating that the flight was close to the nominal one. Considering the flight re-entry as input, a typical result of the ATDB is shown Figure 13. Assuming partial catalytic wall, the temperature evolution along the symmetry line of the vehicle from M= 25 up to the recovery interface is presented.

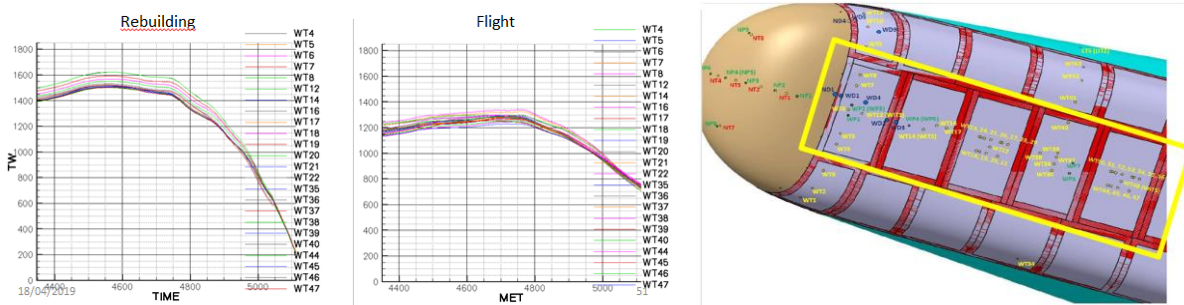


Figure 13: ATDB – flight reconstruction – symmetry line

First of all, no boundary layer transition, at least for this area, is noticed on the flight data. In addition, it is observed that the ATDB over-estimates of about 200°K the general temperature level observed in flight. Assuming flight data as a “reference”, this behaviour is due to margin and uncertainties integrated within the ATDB, like Steps and Gaps overheating, CFD-CFD and CFD-WTT uncertainties. A part of the deviation is also due to the radiative equilibrium assumption at wall for ATDB, without any cooling effect, thermal inertia or conduction-diffusion effect in the TPS material (see Figure 14).

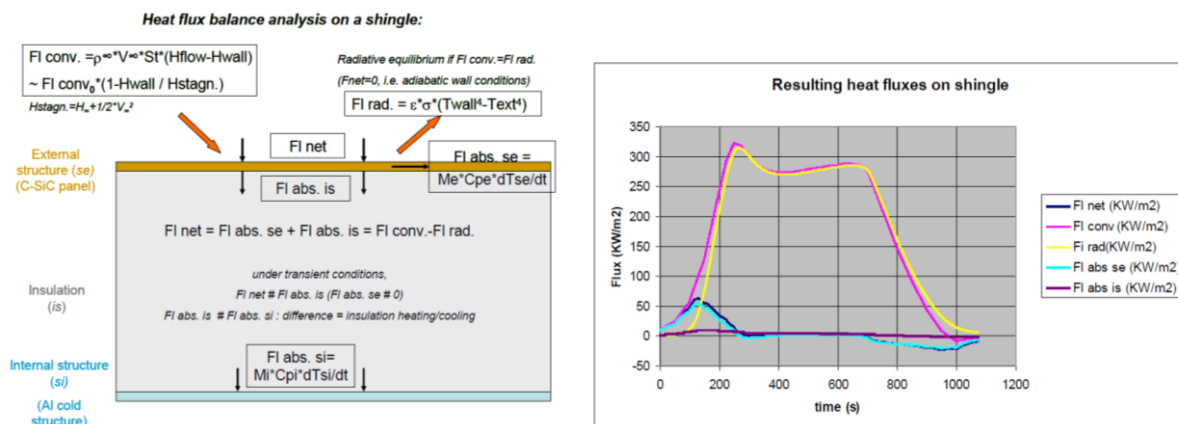


Figure 14: Heat flux balance into a shingle

Some reference re-entry trajectory points were rebuilt by means of CFD (RTECH, CFSe contribution) and compared to the flight data. The remaining deviation with flight data is of the order of magnitude of 50°K.

Other points to be addressed are the reliability of the flight re-entry trajectory and in particular local atmospheric density effect, and the temperature measurements reliability by means of thermocouple.

For the first point, it is confirmed that currently, as far aerodynamic is concerned, we are able to provide reliable aerodynamic coefficients compared to the flight one as shown on Figure 15; density can thus be estimated through inertial accelerometric measurements (IMU).

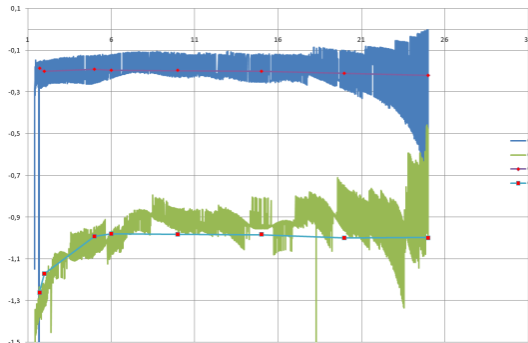


Figure 15: Axial and Normal coefficient - comparison between AEDB and IXV flight vs. Mach

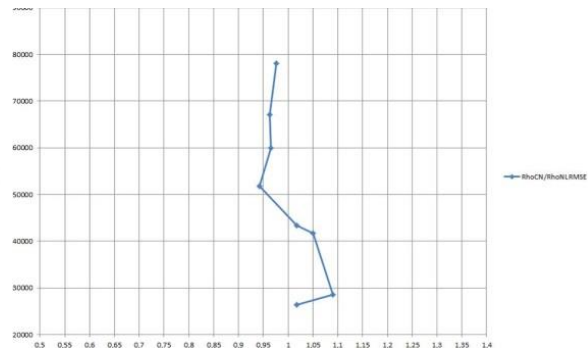


Figure 16: Ratio between density from IMU and density from NRLMSISE-00 atmospheric model vs. altitude

The NRLMSISE-00 atmospheric model combined with GPS information was selected to determine local density for each re-entry trajectory point. The local density from IMU compared with density from NRLMSISE-00 is around 5% lower (see Figure 16) leading to slightly lower heat fluxes.

For the second point and thanks to the In-Flight Experimental plan, advanced Infra-Red camera experiment spotting the leeward side of the flap provided alternate method to the thermocouples to obtain local temperatures. The Figure 17 shows a preliminary result for M=15 which is close to the hottest trajectory point during the flight.

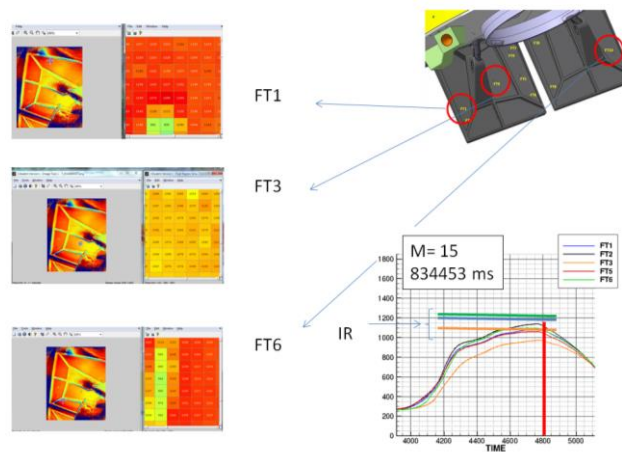


Figure 17: IR experiment – thermocouple comparisons - left flap leeward side

The ATD activities are going on and the current results will be refined and confirmed prior to be used to update the margins policy to be applied to Space Rider Program.

3. Conclusion

Aerodynamic studies performed during previous phase A/B1 and current phase B2/C of Space Rider program have allowed to demonstrate that IXV aeroshape “as-it-is” was capable of flying safely through transonic and subsonic regime at a very high Angle-of-Attack profile (AoA), thus able to fulfill Space Rider mission requirements. Aerodynamic characterization in the range Mach = 1.4 down to Mach = 0.6 has been completed through WTT in INCAS trisonic facility, in order to validate flying qualities and controllability in the transonic flight domain for both longitudinal and lateral behaviors.

Regarding Aerothermodynamics, preparatory activities dealing with IXV post-flight analyses is going on enabling to review and update the margins policy to be applied. Based on the comparison with IXV flight data, no boundary layer transition was observed in flight. The ATDB including margins and uncertainties exhibits a deviation with flight data of around 100°K for the general heat flux. Such deviation is higher than 50°K based on CFD rebuilding. It is to be noticed that the steps and gaps stayed within the requirement all along the IXV flight. Complementary analyses integrating the TPS material interaction (ie: diffusion-conduction) will be performed having as goal to explain the remaining temperature offset between prediction and flight.

3. Acknowledgment

The authors would like to express their appreciation to ESA, TASI, CFSE, RTECH, VKI and INCAS for their expertise and support all along the present activities.

Space Rider is a project of the European Space Agency, where Thales Alenia Space Italy and AVIO SpA are the co-Primes.

Acronyms

AEDB	Aerodynamic Data Base
AoA	Angle of Attack
AoS	Angle of Sideslip
ATDB	AeroThermodynamic Data Base
CFD	Computational Fluid Dynamics
DRS	Descent and Recovery System
ESA	European Space Agency
FQA	Flying Qualities Analysis
GNC	Guidance Navigation and Control
IFE	In-Flight Experiment
IMU	Inertial Measurements Unit
IR	Infra-Red
IXV	Intermediate eXperimental Vehicle
SWBLI	Shock Wave Boundary Layer Interaction
TAS-I	Thales Alenia Space Italy
TPS	Thermal Protection System
WTT	Wind Tunnel Tests

References

- [1] Intermediate Experimental Vehicle, ESA programme – Aerodynamics – Aerothermodynamics and In Flight Experiments A System loop for validating the design tools and for mastering the aerothermodynamics phenoma, ‘Dutheil S, Dembinska F, Tran D, Vallée J-J, Bucalo H, Cantinaud O, Tribot J-P, Mareschi V, Farrerella, Camarri F, Rufolo G, Mancuso S’, 4th EUCASS conference, July 3rd to 10th 2011 St Petersburg, Russia
- [2] Intermediate Experimental Vehicle, ESA program Aerothermodynamics – Transition and Steps and Gaps assessment, ‘Vérant J-L, Pelissier C, Sourgen F, Fontaine J, Garçon F, Spel M, van Hauwaert P, Charbonnier D, Vos J, Vallée J-J, Pibarot J, Tribot J-P, Mareschi V, Farrerella D, Rufolo G’, 7th European symposium on Aerothermodynamics, May 9th to 12th 2011, Brugge, Belgium
- [3] Characterization of the IXV thermal protection system in high enthalpy plasma flow, ‘Panerai F, Helber B, Sakraker I, Pichon T, Barreateau T, Tribot J-P, Vallée J-J, Mareschi V, Farrerella D, Rufolo G, Mancuso S’, 7th European symposium on Aerothermodynamics, May 9th to 12th 2011, Brugge, Belgium
- [4] Intermediate Experimental Vehicle, ESA program Supersonic Transonic Aerodynamics, ‘Sjörs K, Olsson J, Maseland H, de Cock K, Dutheil S, Bouleuc L, Cantinaud O, Tribot J-P, Mareschi V, Farrerella D, Rufolo G’, 7th European symposium on Aerothermodynamics, May 9th to 12th 2011, Brugge, Belgium
- [5] Intermediate Experimental Vehicle, Extrapolation Ground to Flight Experimental and CFD approach, ‘Tribot J-P, Dutheil S, Viguier P, Vérant J-L, Van Hauwaert P, Spel M, Charbonnier D, Vos J, Mareschi V, Ferrarella D, Rufolo G’, IAC 2013, September 23rd to 29th 2013 Beijing, China